

# Diversifying NMR Supersequences with New HSQC-Based Modules

Jonathan R. J. Yong,<sup>1</sup> Ēriks Kupče,<sup>2</sup> Tim D. W. Claridge<sup>1,\*</sup>

<sup>1</sup> *Chemistry Research Laboratory, Department of Chemistry, University of Oxford, Mansfield Road, Oxford, OX1 3TA, U.K.*

<sup>2</sup> *Bruker UK Ltd., Banner Lane, Coventry, CV4 9GH, U.K.*

\* tim.claridge@chem.ox.ac.uk

## Abstract

The sensitivity-enhanced HSQC, as well as HSQC-TOCSY, experiments can be incorporated into NOAH (NMR by Ordered Acquisition using <sup>1</sup>H detection) supersequences. Importantly, these heteronuclear modules preserve the magnetisation required for subsequent acquisition of other homonuclear modules in the supersequence. With these new modules, we reach a total of over 600 practically applicable NOAH supersequences which yield high-quality 2D spectra with greatly reduced experiment durations.

## Introduction

In recent years, there has been significant interest in techniques which accelerate the acquisition of NMR data, especially for multidimensional spectra.<sup>1–3</sup> Some of the more readily implemented approaches involve the use of multiple-FID acquisitions, using either single or multiple receivers. Of these, one of the most versatile approaches is to utilise different “pools” of magnetisation for the sequential collection of different spectra without an intervening recovery delay, as illustrated by the NOAH (NMR by Ordered Acquisition using <sup>1</sup>H detection) technique.<sup>4</sup> Virtually all of the most common 2D experiments used in small molecule characterisation, such as HMBC, HSQC, COSY, NOESY, and TOCSY, can be concatenated in a modular fashion to form *supersequences* which collectively use only one recovery delay ( $d_1$ ) (Figure 1a). As the recovery delay accounts for the

large majority of experiment time in 2D NMR, the NOAH approach can provide time savings of up to  $\sim 4\times$  compared to the conventional individual acquisition of each spectrum, in which each constituent experiment would have its own recovery delay.

One-bond heteronuclear correlation experiments, namely HMQC and HSQC, play a central role in the structural elucidation of small organic molecules and biomolecules.<sup>5</sup> These experiments are also a core component of many NOAH experiments, since the magnetisation they use (protons directly coupled to dilute nuclei, i.e. <sup>13</sup>C or <sup>15</sup>N) can be efficiently differentiated from the “bulk” magnetisation of protons that are not directly attached to these NMR-active nuclei (herein referred to as uncoupled protons).<sup>4d,6</sup> At the same time, due to the low natural abundance of these heteronuclei, these spectra are typically less sensitive than the homonuclear spectra that are placed towards the end of the supersequence. Consequently, for dilute samples, the minimum experimental time is generally dictated by these heteronuclear experiments. Any improvements in experiment sensitivity can be translated into greater time savings.

In the 1990s, Cavanagh, Rance, and Kay introduced the sensitivity-enhanced HSQC (seHSQC) experiment, which improves on the sensitivity of an ordinary echo-antiecho HSQC by up to a factor of 2.<sup>7</sup> This is accomplished by converting two magnetisation components that are cosine- and sine-modulated in  $t_1$  into observable magnetisation prior to detection, in the so-called preservation of equivalent pathways (PEP) scheme. Here, we show how the original seHSQC sequence can be modified such that it can be used as a NOAH module. We add further diversification by introducing a HSQC-TOCSY module, derived from the ASAP-HSQC-TOCSY,<sup>8</sup> that is also compatible with the NOAH strategy. Both of these modules can be inserted either independently or together into NOAH supersequences, allowing large amounts of chemical information to be acquired in short times.

## **<sup>13</sup>C seHSQC**

The NOAH-4 MSCN experiment (Figure 1a) is an example of a NOAH supersequence, which yields <sup>15</sup>N HMQC, <sup>13</sup>C HSQC, COSY, and NOESY spectra in one single experiment. The implemen-

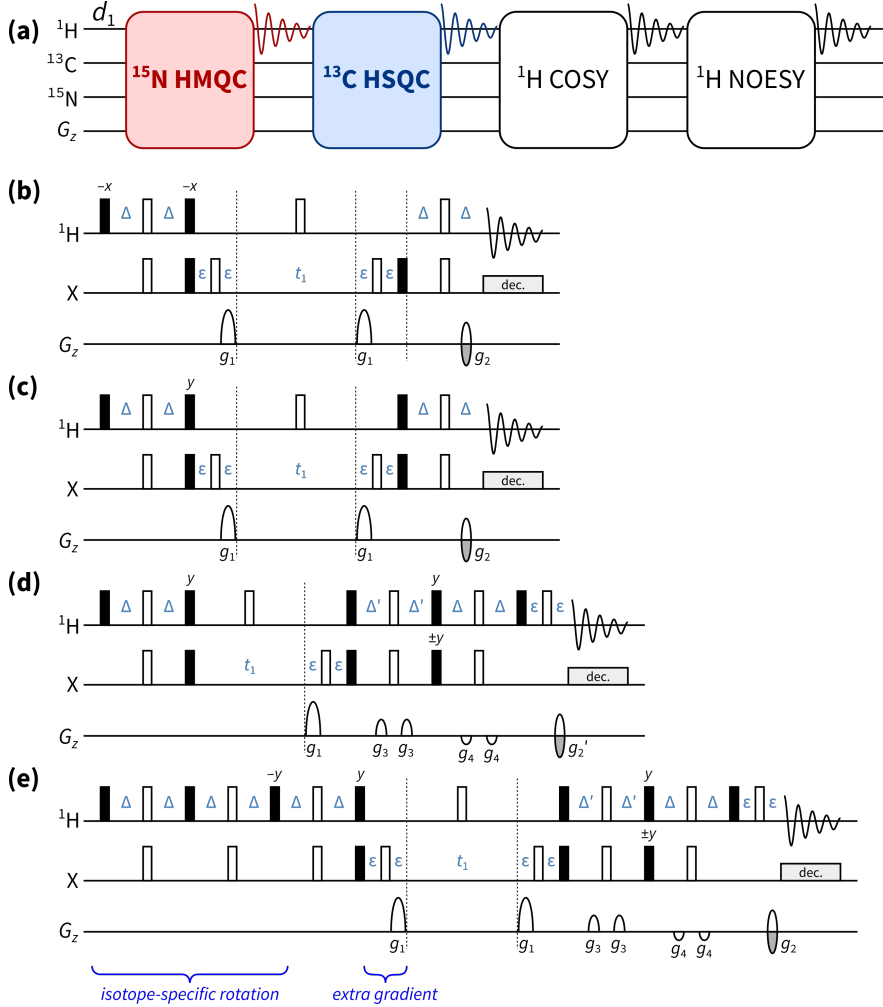


*Figure 1:* (a) Overview of a typical NOAH supersequence (MSCN, using the single-letter abbreviations previously defined<sup>4a</sup>). The <sup>15</sup>N–<sup>1</sup>H HMQC and <sup>13</sup>C–<sup>1</sup>H HSQC modules are highlighted: these may be replaced with the new seHSQC module proposed in this work. (b) Original NOAH HMQC module,<sup>4a,9</sup> abbreviated as “M”. (c) Original NOAH HSQC module without sensitivity enhancement,<sup>4a,10</sup> abbreviated as “S”. (d) Cavanagh–Rance–Kay (CRK) seHSQC.<sup>7</sup> (e) NOAH seHSQC module, abbreviated as “Sp” (this work). Filled and unfilled bars represent 90° and 180° pulses respectively; all 180° pulses on <sup>13</sup>C are adiabatic (swept-frequency) pulses. All pulses are applied along +x unless otherwise noted. The delays are chosen as follows:  $\Delta = 1/(4 \cdot ^1J_{\text{NH}})$ ,  $\Delta' = 1/(8 \cdot ^1J_{\text{CH}})$  or  $1/(4 \cdot ^1J_{\text{NH}})$ , and  $\varepsilon$  is the minimum time needed for a gradient and subsequent recovery. All gradients are 1 ms long, except for  $g_1$  and  $g_2$  in <sup>15</sup>N experiments which are 2.5 ms long. Gradient amplitudes, as percentages of maximum gradient strength, are as follows:  $g_1 = 80\%$ ;  $g_2 = \pm 40.2\%$  (<sup>13</sup>C) or  $\pm 16.2\%$  (<sup>15</sup>N);  $g_2' = g_2/2$ ;  $g_3 = 11\%$ ;  $g_4 = -5\%$ . The signs of  $g_2$  and  $g_2'$  are alternated in each  $t_1$  increment to provide echo–antiecho selection. Refer to Figure S1 for product operator analysis.

tation of this supersequence relies on the fact that the output of any one module contains all the necessary magnetisation components required for downstream modules. For example, both the standard NOAH HMQC (Figure 1b) and HSQC (Figure 1c) modules return the bulk magnetisation

back to its equilibrium position ( $+z$ ). In the MSCN sequence, this bulk magnetisation can therefore be used as the input to the COSY and NOESY homonuclear modules which follow. However, the original Cavanagh–Rance–Kay (CRK) seHSQC (Figure 1d) does not obey this principle: it causes bulk magnetisation to be dephased by coherence transfer pathway (CTP) gradients. Consequently, downstream modules can only utilise any bulk magnetisation that has relaxed during the HSQC FID acquisition, leading to drastic losses in signal intensity. This is illustrated using a NOAH-2 SpCc (seHSQC + CLIP-COSY<sup>11</sup>) supersequence (Figure 2a): while the CRK seHSQC implementation afford significant sensitivity gains (primarily for CH peaks, as predicted by theory<sup>12</sup>), the COSY module which follows suffers from an almost complete loss of intensity.

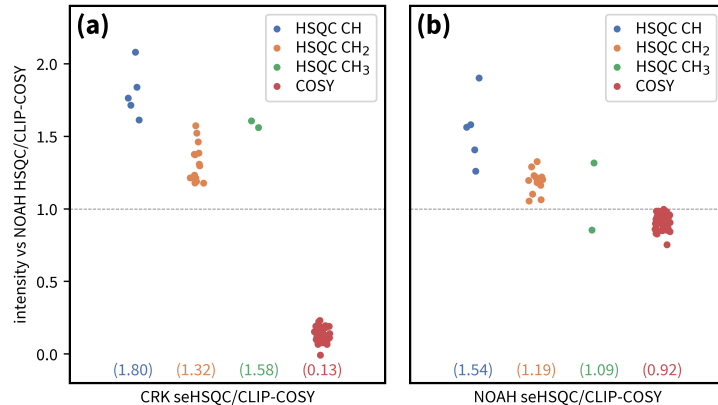


*Figure 2: [We could add spectra here? I think the graph is the most important piece of information, but I'm sure people like to see spectra more than graphs...]* Sensitivity comparisons for NOAH-2 SpCc (seHSQC + CLIP-COSY) supersequences, using the CRK (Figure 1d) and NOAH (Figure 1e) seHSQC implementations. All intensities are normalised against the NOAH-2 SCc (HSQC + CLIP-COSY) supersequence, without HSQC sensitivity enhancement. HSQC intensities are further grouped by multiplicity. Numbers in parentheses indicate averages over all peaks of a given type. (a) Using the original CRK seHSQC. The CRK seHSQC does not preserve the bulk magnetisation, leading to severely reduced COSY intensities. (b) Using the NOAH seHSQC. Spectra were obtained on a 700 MHz Bruker AV III equipped with a TCI H/C/N cryoprobe; the sample used was 40 mM andrographolide in DMSO-*d*<sub>6</sub>.

Our solution is based on the simple observation that the bulk magnetisation in the seHSQC will be returned to  $+z$  if the phase of the initial  $^1\text{H}$  90° pulse is changed by 90° to  $+y$ . To generate the HSQC signal, however, the same pulse needs to be applied along  $+x$ . Overall, what is required is therefore a pulse sequence element which simultaneously acts as a 90°<sub>*x*</sub> (or 90°<sub>*-x*</sub>) pulse on protons coupled to  $^{13}\text{C}$ , and as a 90°<sub>*y*</sub> pulse on uncoupled protons. We accomplish this by prepending a

double heteronuclear spin echo, which we refer to as the *isotope-specific rotation* (ISR), to the pulse sequence. It is similar to the *zz*-filter, which we have previously used in the NOAH HMBC module to retain the magnetisation of directly coupled protons for a subsequent HSQC module.<sup>4b,4d</sup> However, the ISR has different pulse phases to this and consequently leads to a different overall outcome. While the BIG-BIRD element developed by Briand and Sørensen<sup>13</sup> is also capable of effecting this, we find that the ISR provides greater signal-to-noise in both the seHSQC itself, as well as downstream modules (Figure S5).

In addition to the ISR, the NOAH seHSQC module also contains a CTP gradient prior to the  $t_1$  period (highlighted in Figure 1e). This gradient is not necessary for the seHSQC module itself, but instead serves to suppress artefacts in downstream modules, which would otherwise arise from bulk magnetisation that evolves during either half of the HSQC  $t_1$  period. This then evolves again in the  $t_1$  period of a later homonuclear module (e.g. COSY), resulting in each COSY peak with  $\Omega_1 = \Omega_H$  being accompanied by a pair of “wing” artefacts at  $\Omega_1 = \Omega_H \pm (\Omega_H \cdot SW_C)/(2 \cdot SW_H)$ , which can reach  $\sim 5\%$  of the intensity of their parent peaks. Importantly, the artefacts arising from diagonal peaks can have intensities that are comparable to genuine crosspeaks (Figure S6), which highlights the importance of suppressing these artefacts.

With these modifications, the NOAH seHSQC module provides clear sensitivity gains over the NOAH HSQC module, while preserving essentially the same amount of  $^1H$  magnetisation for downstream modules (Figure 2b). The modifications present in the NOAH seHSQC, particularly the ISR, mean that the sensitivity improvements are slightly lower as compared to the original CRK implementation. On average, CH and  $CH_2$  peaks have  $1.54\times$  and  $1.19\times$  increased sensitivity respectively relative to the NOAH HSQC module. However, a dramatic improvement is seen in the COSY module which follows. In contrast to the CRK seHSQC, which completely destroys the requisite bulk magnetisation, the NOAH seHSQC preserves the majority of it, performing 92% as well as the original HSQC module.

Multiplicity editing can be easily incorporated into the NOAH seHSQC sequence (Figure S2), leading to similar sensitivity gains relative to the HSQC module. It is noteworthy that the original

NOAH HSQC (without sensitivity enhancement) places the bulk magnetisation in the  $xy$ -plane during the  $t_1$  and editing periods, whereas the newly proposed NOAH seHSQC places the bulk along  $\pm z$ . In the former, the bulk magnetisation is therefore subject to homonuclear coupling ( $J_{HH}$ ) evolution, leading to a small decrease in the sensitivity of later homonuclear modules when multiplicity editing is introduced. Since homonuclear experiments typically have a greater inherent sensitivity than the HSQC, this minor loss is not a problem, and is far outweighed by the benefits of incorporating multiplicity editing in the HSQC. Nevertheless, the fact that the seHSQC does not suffer from such a penalty is a welcome benefit. As a result, the edited NOAH seHSQC slightly outperforms the edited HSQC in terms of preserving bulk magnetisation, with subsequent homonuclear modules enjoying a slight boost in sensitivity (Figure S3).

(On second thoughts, I'm wondering if it may not be useful to put ASAP-seHSQC stuff here... Firstly it's a slightly different context and I think there are considerations in ASAP that don't make much sense here – for example use of URPs which helps to clean ASAP spectra up quite a bit but don't see much use here. Secondly – especially given the recent interest in fast-repetition sequences – there might be potential for some of that to be reported elsewhere. We would have to try to make a bit more sense out of various issues first though, such as how useful exactly is mixing vs relaxation, etc...)

## **$^{15}\text{N}$ seHSQC**

The proposed seHSQC module can be similarly implemented for  $^{15}\text{N}$  experiments. Currently, in NOAH supersequences,  $^{15}\text{N}-^1\text{H}$  correlations are primarily obtained using the HMQC module, since this manipulates bulk magnetisation more favourably than the HSQC (*vide infra*).<sup>4a,9</sup> Compared to this, the new seHSQC module can provide greater than  $4\times$  greater sensitivity (Figure 3). This arises partly because of the use of the PEP sensitivity enhancement scheme, in which the reverse? INEPT transfer delays  $\Delta'$  can be optimised for NH peaks. However, there is also a significant improvement due to the fact that peaks in the  $^{15}\text{N}$  seHSQC are not broadened in the indirect dimension by  $J_{HH}$ , unlike in the HMQC. Although the seHSQC retains a slightly smaller amount of bulk magnetisation

( $\sim 70\%$ , versus  $\sim 80\%$  for the HMQC), this is generally not a problem, since it is the  $^{15}\text{N}$  module which typically has the lowest intrinsic sensitivity in a supersequence.

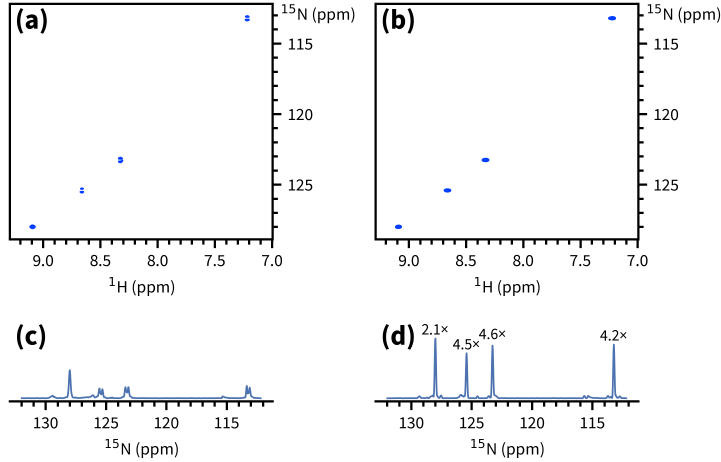


*Figure 3:* Comparison of the new  $^{15}\text{N}-^1\text{H}$  seHSQC with the standard NOAH HMQC module, taken from NOAH-3 XSpCc supersequences ( $^{15}\text{N}$  experiment +  $^{13}\text{C}$  seHSQC + CLIP-COSY). (a)  $^{15}\text{N}$  HMQC spectrum. (b)  $^{15}\text{N}$  seHSQC spectrum. (c) Projection of HMQC onto the  $f_1$  axis. Splitting due to  $J_{\text{HH}}$  is clearly visible for three of the four peaks. (d) Projection of seHSQC onto the  $f_1$  axis. Signal-to-noise improvements relative to the HMQC spectrum are indicated over each peak. The largest gains are observed for peaks where the multiplet structure is collapsed; however, even in the absence of that, a  $\sim 2\times$  gain is still obtained. Spectra were obtained on a 700 MHz Bruker AV III equipped with a TCI H/C/N cryoprobe; the sample used was 40 mM gramicidin in DMSO- $d_6$ .

While a  $^{15}\text{N}$  HSQC module (without sensitivity enhancement) would still benefit from multiplet collapse, it comes with other severe drawbacks. As previously discussed, the HSQC module places bulk magnetisation in the  $xy$ -plane during the  $t_1$  period. Consequently, the amount of bulk magnetisation that is retained decreases as  $t_1$  is lengthened, leading to line broadening in the indirect dimensions of all downstream modules (Figure S7). Whilst this is not a problem with the  $^{13}\text{C}$  HSQC where typical  $^{13}\text{C}$  indirect dimension acquisition times are relatively short, the smaller spectral widths in  $^{15}\text{N}$  experiments can mean downstream modules suffer losses in both sensitivity and resolution. The seHSQC module avoids this issue entirely, making it especially well-suited to obtaining  $^{15}\text{N}$  correlations.

For optimal performance, the  $^{15}\text{N}$  seHSQC module benefits from one notable change with respect to its  $^{13}\text{C}$  counterpart, which is that the CTP gradients  $g_1$  and  $g_2$  (Figure 1e) are all lengthened from a typical duration of 1 ms to 2.5 ms. This is to more effectively dephase any residual bulk

magnetisation that, due to the cumulative effect of pulse imperfections, is transverse just prior to detection. If left uncontrolled, this magnetisation can lead to significant levels of artefacts in the seHSQC module itself (Figure S8). The  $^{13}\text{C}$  seHSQC does not need this gradient extension because of the larger amplitude of  $g_2$ ; however, the corresponding  $^{15}\text{N}$  gradient is weaker by a factor of  $\gamma_{\text{C}}/\gamma_{\text{N}} \approx 2.5$ , thus requiring a longer duration in order to produce comparable artefact attenuation. In practice, we find that gradient durations of 2 to 2.5 ms provide sufficient suppression whilst not causing any appreciable difference in the intensity of the desired crosspeaks (Figure S8).

In scenarios where high resolution in the  $^{15}\text{N}$  dimension is not required, it can prove useful to reduce the number of  $t_1$  increments and in its place increase the number of transients acquired.<sup>2b,14</sup> In new versions of the NOAH pulse programmes (including those provided in the *Supporting Information*), this feature can be enabled by specifying a factor  $k$  by which to perform this scaling. Note that the scaling is only applied to the  $^{15}\text{N}$  module; all other modules are left untouched. In our hands, setting  $k = 2$  or  $4$  for the  $^{15}\text{N}$  HMQC can lead to significant sensitivity gains ([how much?](#)), since  $J_{\text{HH}}$  splitting in the indirect dimension can no longer be resolved ([SI](#)). This point is not relevant to the seHSQC, and here  $k$ -scaling on its own has only a tiny effect on peak height (and signal-to-noise), since any sensitivity gained from the extra transients is offset by the broadening. However, the later  $t_1$  increments which were not acquired can be reconstructed using linear projection ([cite](#)) to mitigate this line broadening. The resulting spectra display sensitivity gains of up to a factor of  $k$ , although the fidelity of the reconstruction suffers for  $k > 4$  ([SI](#)).

## Double HSQC and HSQC-TOCSY

[Need figure](#)

Next, we note that the HSQC module (though not the new seHSQC module) allows an arbitrary amount of  $^{13}\text{C}-^1\text{H}$  magnetisation to be excited, with the remainder returned to  $+z$ . In order to excite a proportion  $f$  of  $^{13}\text{C}-^1\text{H}$  magnetisation ( $0 < f \leq 1$ ), the initial INEPT delay must be shortened by a factor of  $\sin^{-1} f$ . The remaining  $(1 - f)$  of the magnetisation, plus any that recovers during the first HSQC FID, can then be used for a second HSQC module in the same

supersequence. The collection of multiple HSQC spectra in one multi-FID acquisition (MFA) experiment has previously been accomplished by keeping the two CTPs in the CRK seHSQC separate, with the cosine- and sine-modulated CTPs each contributing to one spectrum.<sup>15</sup> However, with a value of  $f = 0.8$ , the NOAH strategy already provides slightly higher sensitivity for both spectra. Furthermore, the sensitivity of the second HSQC can be further boosted by using the new seHSQC module in place of it (SI).

By adding a period of isotropic mixing prior to detection, the NOAH HSQC module may be converted to a HSQC-TOCSY module. This is similar to the previously reported ASAP-HSQC-TOCSY,<sup>8</sup> the key difference being that in the present NOAH context, unused  $^{13}\text{C}$ - $^1\text{H}$  and bulk magnetisation is preserved for use in other modules, instead of later  $t_1$  increments as in the ASAP experiment. Compared to the existing MFA HSQC-TOCSY/HSQC experiment,<sup>15a</sup> our approach has several characteristics which make it particularly amenable to use in NOAH supersequences. Firstly, the vast majority of bulk magnetisation is preserved, as required for homonuclear module(s) to be appended in a NOAH supersequence (in practice, losses of ca. 10% are observed due to pulse imperfections). In contrast, the MFA sequence, much like the original CRK seHSQC on which it is based, dephases bulk magnetisation and causes a 80–90% sensitivity loss in downstream spectra. Secondly, the sensitivity of both spectra in a NOAH experiment can be optimised through the value of  $f$ ; this allows a larger amount of  $^{13}\text{C}$ - $^1\text{H}$  magnetisation to be used for the inherently less sensitive HSQC-TOCSY (in our experience, setting  $f = 0.9$  provides a good balance). Lastly, since each NOAH module is independently executed, the NOAH approach allows multiplicity editing to be enabled for only the HSQC and not the HSQC-TOCSY, where accidental overlap may lead to crosspeaks being lost unexpectedly.

Despite these benefits, we note that it is not possible to simply insert a TOCSY mixing block into the seHSQC module presented here, as that will lead to the bulk magnetisation being dephased. Therefore, the NOAH HSQC-TOCSY module will still have lower overall sensitivity than a conventional seHSQC-TOCSY, which can make use of the PEP scheme.

(I removed the bit on fast acquisition being most useful for concentrated samples. We can add back

later if needed.)

## Example spectra and conclusion

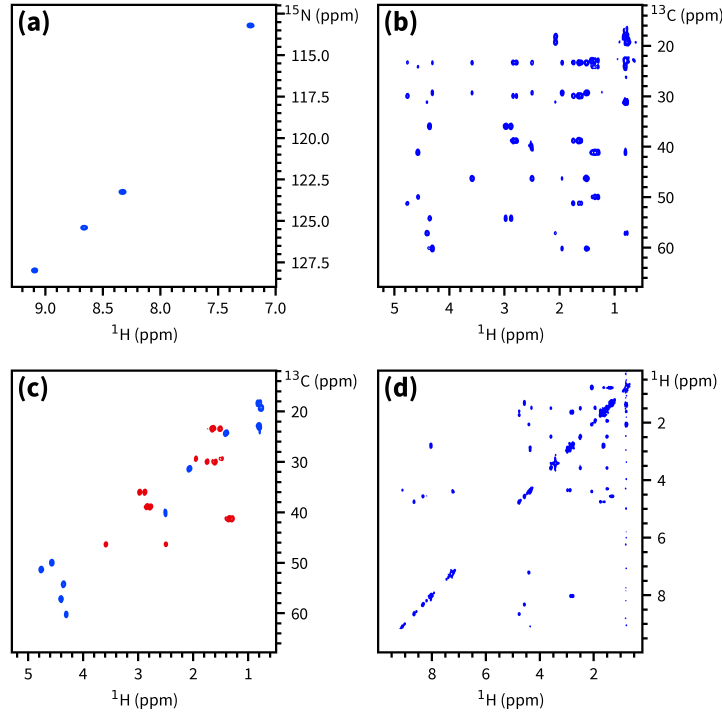


*Figure 4:* Example spectra obtained from the NOAH-4 SpStSpCc supersequence. 256  $t_1$  increments were used, with 2 scans per increment. The total experiment time was 17 minutes and 35 seconds. (a)  $^{15}\text{N}$  seHSQC. (b)  $^{13}\text{C}$  HSQC-TOCSY ( $f = 0.9$ ). (c) Multiplicity-edited  $^{13}\text{C}$  seHSQC. Notice that having the edited seHSQC removes the need for the less desirable HSQC-TOCSY editing. (d) CLIP-COSY. Spectra were obtained on a 700 MHz Bruker AV III equipped with a TCI H/C/N cryoprobe; the sample used was 40 mM gramicidin in DMSO- $d_6$ .

The NOAH-4 SpStSpCc ( $^{15}\text{N}$  seHSQC,  $^{13}\text{C}$  HSQC-TOCSY,  $^{13}\text{C}$  seHSQC, and CLIP-COSY) supersequence is one of many ways in which the new modules discussed above can be included in practical experiments. The spectra thus obtained are shown in Figure 4. While individual collection of the four spectra above would require 57 minutes and 8 seconds, the NOAH-4 supersequence takes only 17 minutes and 35 seconds, which represents a  $3.25\times$  speedup. One can also prepend the NOAH HMBC module (“B”);<sup>4d</sup> this uses the semi-adiabatic  $zz$ -filter to preserve magnetisation of protons directly coupled to  $^{13}\text{C}$  and  $^{15}\text{N}$  heteronuclei, which is precisely the magnetisation required

by the HSQC-based modules presented here. In particular, supersequences such as the NOAH-4 BStSpC allow the rapid and complete collection of C–H and H–H correlations for typical organic molecules. Examples of such spectra, with time savings of up to  $3.8\times$ , are shown in the *Supporting Information (SI)*.

The new seHSQC and HSQC-TOCSY implementations add to the preexisting diversity in NOAH modules, bringing the total number of plausible NOAH supersequences to over 600. The AU scripts needed for processing of these modules, as well as a number of the more commonly used pulse sequences, are provided in the *Supporting Information*; others are available upon request from the authors. However, a more user-friendly and customisable method for the generation of NOAH pulse sequences is clearly needed to handle the sheer variety currently available. Our work towards this will be reported in the near future.

## Acknowledgements

J.R.J.Y. thanks the Clarendon Fund (University of Oxford) and the EPSRC Centre for Doctoral Training in Synthesis for Biology and Medicine (EP/L015838/1) for a studentship, generously supported by AstraZeneca, Diamond Light Source, Defence Science and Technology Laboratory, Evotec, GlaxoSmithKline, Janssen, Novartis, Pfizer, Syngenta, Takeda, UCB, and Vertex. [Any other acknowledgements?](#)

## References

1. (a) Frydman, L.; Scherf, T.; Lupulescu, A. *Proc. Natl. Acad. Sci. U. S. A.* **2002**, *99*, 15858–15862; (b) Frydman, L.; Lupulescu, A.; Scherf, T. *J. Am. Chem. Soc.* **2003**, *125*, 9204–9217.
2. (a) Nolis, P.; Pérez-Trujillo, M.; Parella, T. *Angew. Chem. Int. Ed.* **2007**, *46*, 7495–7497; (b) Parella, T.; Nolis, P. *Concepts Magn. Reson.* **2010**, *36A*, 1–23.
3. (a) Kupče, Ě.; Freeman, R.; John, B. K. *J. Am. Chem. Soc.* **2006**, *128*, 9606–9607; (b) Kovacs, H.; Kupče, Ě. *Magn. Reson. Chem.* **2016**, *54*, 544–560.

4. (a) Kupče, Ě.; Claridge, T. D. W. *Angew. Chem. Int. Ed.* **2017**, *56*, 11779–11783; (b) Kupče, Ě.; Claridge, T. D. W. *Chem. Commun.* **2018**, *54*, 7139–7142; (c) Claridge, T. D. W.; Mayzel, M.; Kupče, Ě. *Magn. Reson. Chem.* **2019**, *57*, 946–952; (d) Kupče, Ě.; Claridge, T. D. W. *J. Magn. Reson.* **2019**, *307*, 106568.
5. (a) Claridge, T. D. W., *High-Resolution NMR Techniques in Organic Chemistry*, 3rd ed.; Elsevier: Amsterdam, 2016; (b) Cavanagh, J., *Protein NMR Spectroscopy: Principles and Practice*, 2nd ed.; Academic Press: Burlington, Mass., 2007.
6. Garbow, J. R.; Weitekamp, D. P.; Pines, A. *Chem. Phys. Lett.* **1982**, *93*, 504–509.
7. (a) Palmer, A. G.; Cavanagh, J.; Wright, P. E.; Rance, M. *J. Magn. Reson.* **1991**, *93*, 151–170; (b) Kay, L.; Keifer, P.; Saarinen, T. *J. Am. Chem. Soc.* **1992**, *114*, 10663–10665; (c) Cavanagh, J.; Rance, M. *Annu. Rep. NMR Spectrosc.* **1993**, *27*, 1–58.
8. Becker, J.; Koos, M. R. M.; Schulze-Sünninghausen, D.; Luy, B. *J. Magn. Reson.* **2019**, *300*, 76–83.
9. Kupče, Ě.; Freeman, R. *Magn. Reson. Chem.* **2007**, *45*, 2–4.
10. Schulze-Sünninghausen, D.; Becker, J.; Koos, M. R. M.; Luy, B. *J. Magn. Reson.* **2017**, *281*, 151–161.
11. Koos, M. R. M.; Kummerlöwe, G.; Kaltschnee, L.; Thiele, C. M.; Luy, B. *Angew. Chem. Int. Ed.* **2016**, *55*, 7655–7659.
12. (a) Schleucher, J.; Schwendinger, M.; Sattler, M.; Schmidt, P.; Schedletzky, O.; Glaser, S. J.; Sørensen, O. W.; Griesinger, C. *J. Biomol. NMR* **1994**, *4*, 301–306; (b) Kontaxis, G.; Stonehouse, J.; Laue, E. D.; Keeler, J. *J. Magn. Reson.* **1994**, *111*, 70–76.
13. Briand, J.; Sørensen, O. W. *J. Magn. Reson.* **1997**, *125*, 202–206.
14. Pérez-Trujillo, M.; Nolis, P.; Bermel, W.; Parella, T. *Magn. Reson. Chem.* **2007**, *45*, 325–329.
15. (a) Nolis, P.; Motiram-Corral, K.; Pérez-Trujillo, M.; Parella, T. *ChemPhysChem* **2019**, *20*, 356–360; (b) Nolis, P.; Motiram-Corral, K.; Pérez-Trujillo, M.; Parella, T. *J. Magn. Reson.* **2019**, *300*, 1–7.

Supporting Information  
*for*  
Diversifying NOAH Supersequences with New  
HSQC-based Modules

Jonathan R. J. Yong,<sup>1</sup> Ēriks Kupče,<sup>2</sup> Tim D. W. Claridge<sup>1,\*</sup>

<sup>1</sup> *Chemistry Research Laboratory, Department of Chemistry, University of Oxford,  
Mansfield Road, Oxford, OX1 3TA, U.K.*

<sup>2</sup> *Bruker UK Ltd., Banner Lane, Coventry, CV4 9GH, U.K.*

\* tim.claridge@chem.ox.ac.uk

## Contents

<b>1 Product operator analysis for NOAH modules</b>	<b>S3</b>
<b>2 Multiplicity editing in seHSQC</b>	<b>S4</b>
<b>3 Effect of setting <math>\Delta' = 1/(4 \cdot {}^1J_{\text{CH}})</math> in seHSQC</b>	<b>S5</b>
<b>4 Comparison of BIG-BIRD and ISR elements</b>	<b>S6</b>
<b>5 Suppression of wing artefacts</b>	<b>S7</b>
<b>6 <math>{}^{15}\text{N}</math> HSQC and line broadening</b>	<b>S8</b>
<b>7 Effect of lengthened gradients in <math>{}^{15}\text{N}</math> experiments</b>	<b>S9</b>
<b>8 Effect of <math>k</math>-scaling</b>	<b>S10</b>
<b>9 HSQC-TOCSY/HSQC sensitivity comparisons</b>	<b>S13</b>
<b>10 Other example spectra</b>	<b>S15</b>
<b>11 Pulse programmes</b>	<b>S16</b>
<b>12 Processing scripts</b>	<b>S17</b>

# 1 Product operator analysis for NOAH modules

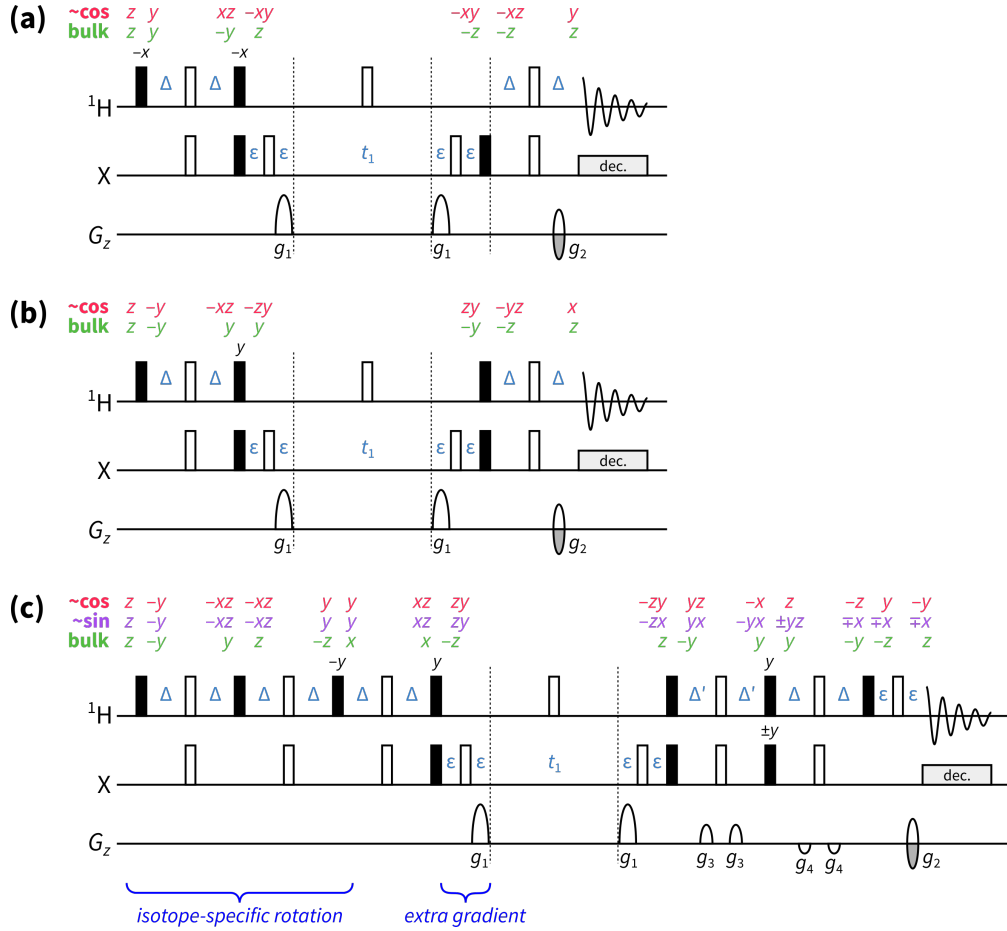


*Figure S1:* Product operators present at each stage of NOAH modules for an IS spin system. One-letter terms  $m$  ( $m \in \{x, y, z\}$ ) are shorthand for single-spin terms on proton, i.e.  $\hat{I}_m$ . Two-letter terms  $mn$  are shorthand for two-spin terms on both the proton and heteronucleus, i.e.  $2\hat{I}_m\hat{S}_n$ . “ $\sim\cos$ ” represents the pathway for directly coupled proton magnetisation that is cosine-modulated after  $t_1$ : for the HMQC and HSQC, this is the only component that is detected. For the seHSQC, the sine-modulated component (labelled with “ $\sim\sin$ ”) is also detected. “bulk” refers to the bulk magnetisation, i.e. protons that are not directly coupled to the heteronucleus. **(a)** NOAH HMQC. **(b)** NOAH HSQC. **(c)** NOAH seHSQC with ISR. Immediately following the ISR pulse sequence element, directly bonded protons are rotated onto  $+y$ , whereas the bulk magnetisation is rotated onto  $+x$ . Note that this analysis assumes  $\Delta' = 1/(4 \cdot {}^1J_{\text{XH}})$ .

## 2 Multiplicity editing in seHSQC

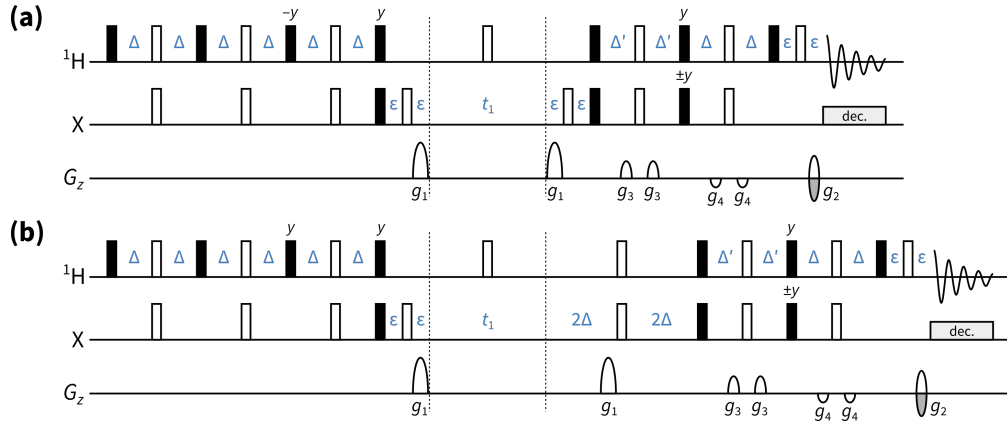


*Figure S2:* Implementation of multiplicity editing in the new NOAH seHSQC module. (a) Unedited NOAH seHSQC, as presented in the main text. (b) Edited NOAH seHSQC (note the different phase in the third  $^1\text{H}$  90° pulse; this is needed to compensate for the extra 180° in the editing period). Symbols have the same meaning as in Figure 1 of the main text.

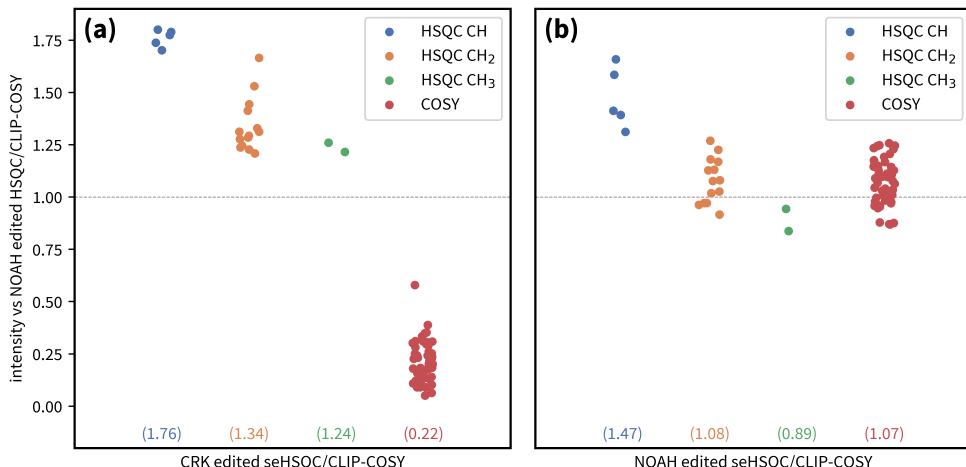


*Figure S3:* Sensitivity of edited seHSQC versus the NOAH HSQC/CLIP-COSY supersequence. (a) CRK edited seHSQC + CLIP-COSY. Although larger gains are observed in the HSQC, the COSY intensities are severely decreased. (b) NOAH edited seHSQC + CLIP-COSY. On average, sensitivity gains are observed in both the HSQC and COSY modules (except for HSQC CH<sub>3</sub> peaks). Spectra were obtained on a 700 MHz Bruker AV III equipped with a TCI H/C/N cryoprobe; the sample used was 40 mM andrographolide in DMSO-*d*<sub>6</sub>.

### 3 Effect of setting $\Delta' = 1/(4 \cdot {}^1J_{CH})$ in seHSQC

The  $\Delta'$  delay in the CRK and NOAH seHSQC sequences can be set to  $1/(4 \cdot {}^1J_{CH})$  in order to optimise the sensitivity enhancement for CH groups only. The effects of doing so are shown here for the unedited and edited seHSQCs respectively.

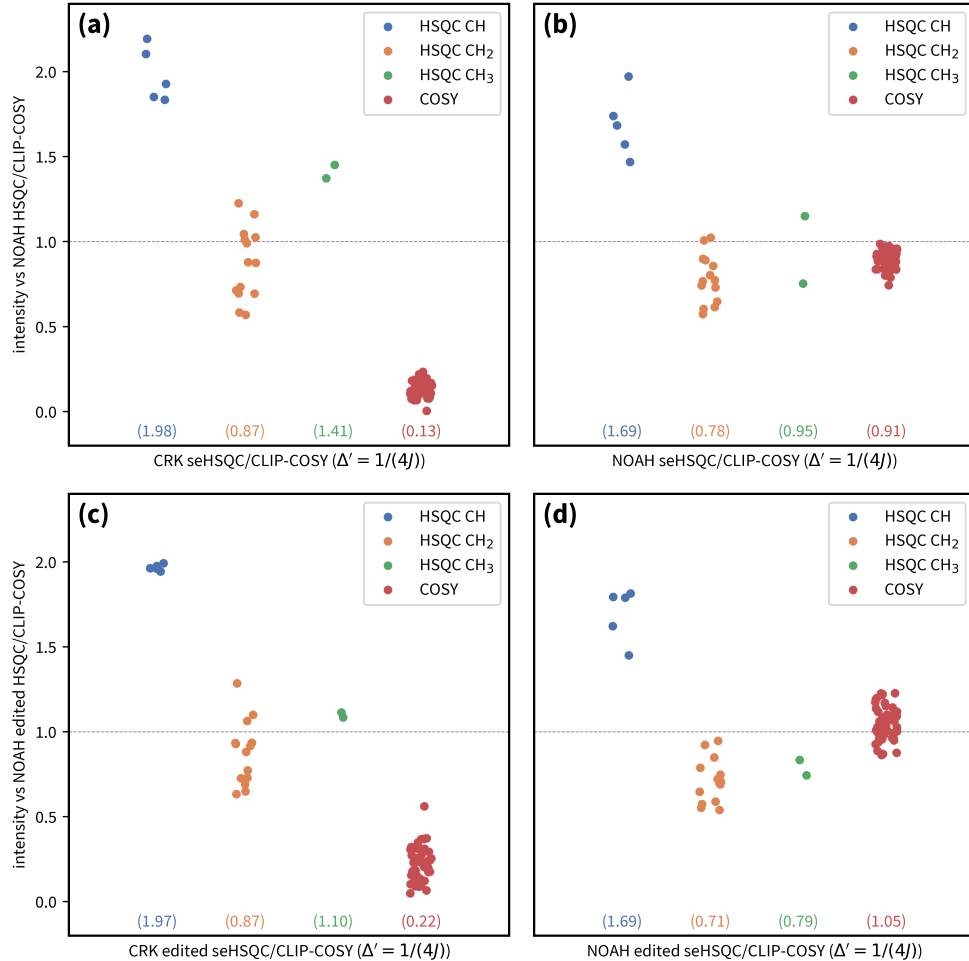
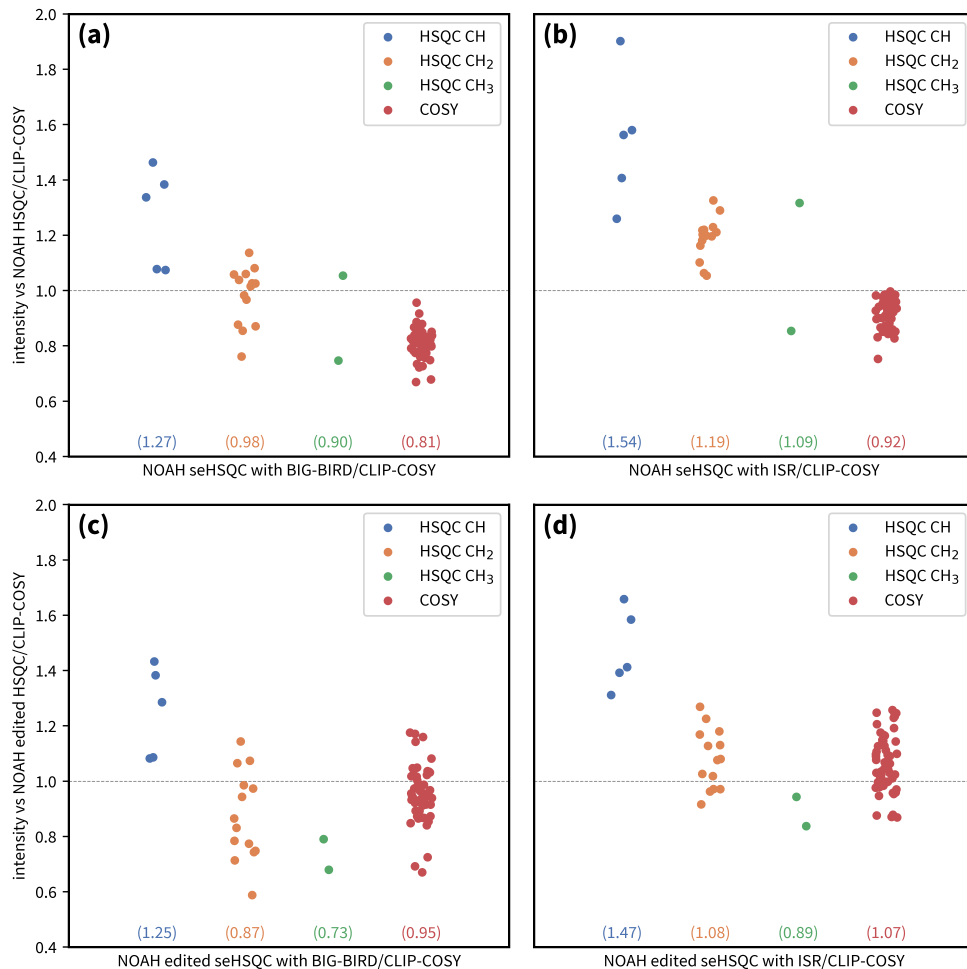


Figure S4: Sensitivity of seHSQC sequences with  $\Delta'$  set to  $1/(4 \cdot {}^1J_{CH})$ , versus the corresponding NOAH HSQC/CLIP-COSY supersequence (i.e. unedited for (a) and (b), edited for (c) and (d)). (a) CRK seHSQC + CLIP-COSY, without multiplicity editing. (b) NOAH seHSQC + CLIP-COSY, without multiplicity editing. (c) CRK seHSQC + CLIP-COSY, with multiplicity editing. (d) NOAH seHSQC + CLIP-COSY, with multiplicity editing. Spectra were obtained on a 700 MHz Bruker AV III equipped with a TCI H/C/N cryoprobe; the sample used was 40 mM andrographolide in DMSO-*d*<sub>6</sub>.

In particular, for the NOAH seHSQC, we note that the improvements in HSQC CH sensitivity gained by moving from  $\Delta' = 1/(8 \cdot {}^1J_{CH})$  to  $\Delta' = 1/(4 \cdot {}^1J_{CH})$  are marginal (ca. 10%). At the same time, sensitivity *losses* are observed for CH<sub>2</sub> and CH<sub>3</sub> peaks, likely due to pulse imperfections.

## 4 Comparison of BIG-BIRD and ISR elements

The BIG-BIRD element used here was  $45^\circ_{45^\circ}(^1\text{H}) - 2\Delta - 180^\circ(^1\text{H}, ^{13}\text{C}) - 2\Delta - 45^\circ_{225^\circ}(^1\text{H})$  for the unedited NOAH seHSQC, where  $\beta_\phi$  indicates a hard pulse with flip angle  $\beta$  and phase  $\phi$ , and  $\Delta = 1/(4 \cdot ^1\text{J}_{\text{CH}})$ . For the edited NOAH seHSQC, the BIG-BIRD pulse phases are slightly modified to give  $45^\circ_{315^\circ}(^1\text{H}) - 2\Delta - 180^\circ(^1\text{H}, ^{13}\text{C}) - 2\Delta - 45^\circ_{135^\circ}(^1\text{H})$ . These, and the ISR, have the same net effect on coupled and uncoupled proton magnetisation, as shown in Figure S1. However, the ISR provides greater sensitivity in both the HSQC and downstream COSY.



*Figure S5:* Sensitivity of NOAH seHSQC sequences with prepended BIG-BIRD and ISR elements, versus the corresponding NOAH HSQC/CLIP-COSY supersequence (i.e. unedited for (a) and (b), edited for (c) and (d)). (a) NOAH seHSQC with BIG-BIRD + CLIP-COSY, without multiplicity editing. (b) NOAH seHSQC with ISR + CLIP-COSY, without multiplicity editing. (c) NOAH seHSQC with BIG-BIRD + CLIP-COSY, with multiplicity editing. (d) NOAH seHSQC with ISR + CLIP-COSY, with multiplicity editing. Spectra were obtained on a 700 MHz Bruker AV III equipped with a TCI H/C/N cryoprobe; the sample used was 40 mM andrographolide in DMSO-*d*<sub>6</sub>.

## 5 Suppression of wing artefacts

The origin of the “wing” artefacts in the final homonuclear modules can be most clearly seen from the following series of experiments involving the NOAH-3  $^{15}\text{N}$  seHSQC/ $^{13}\text{C}$  seHSQC/CLIP-COSY (SpSpCc) supersequence. Since the  $f_1$  spectral windows of the two seHSQC modules are different, they lead to distinct sets of wing artefacts if the extra gradient before  $t_1$  is not present. Figure S6 focuses on the artefacts associated with intense methyl group peaks, but similar artefacts are observed for all other peaks, albeit with lower absolute intensities.

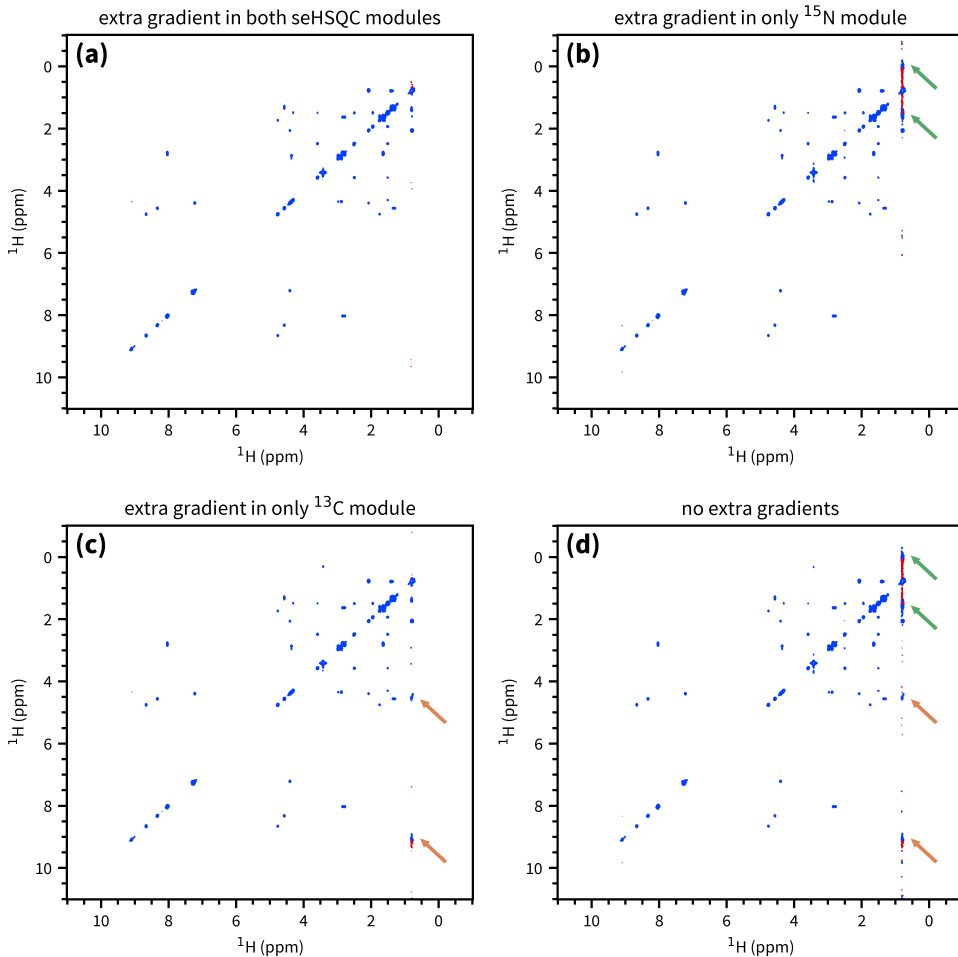


*Figure S6:* CLIP-COSY spectra obtained from various forms of the NOAH-3 SpSpCc supersequence. Wing artefacts arising from the  $^{15}\text{N}$  seHSQC are highlighted in orange; those arising from the  $^{13}\text{C}$  seHSQC in green. Notice how (in this case) the former can easily be misinterpreted as a crosspeak, while the latter obscures genuine crosspeaks. **(a)** With the extra gradient inserted for both modules, i.e. no artefacts. **(b)** With an extra gradient in only the  $^{15}\text{N}$  module, i.e. only the  $^{13}\text{C}$  artefacts. **(c)** With an extra gradient in only the  $^{13}\text{C}$  module. **(d)** With no extra gradients. Spectra were obtained on a 700 MHz Bruker AV III equipped with a TCI H/C/N cryoprobe; the sample used was 40 mM gramicidin in DMSO- $d_6$ .

## 6 $^{15}\text{N}$ HSQC and line broadening

For  $^{15}\text{N}-^1\text{H}$  correlations, both the HMQC and the new seHSQC module are recommended as they keep the bulk magnetisation along  $\pm z$  during the  $t_1$  period. The HSQC module places bulk magnetisation in the  $xy$ -plane, leading to  $J_{\text{HH}}$  evolution; consequently, the amount of bulk magnetisation “passed on” to the downstream modules decreases as the  $^{15}\text{N}$   $t_1$  is increased. Since  $t_1$  for each NOAH module is incremented in sync, this is manifested in downstream modules as a  $t_1$ -dependent decrease in amplitude, or  $f_1$  line broadening after Fourier transformation, as shown in Figure S7.

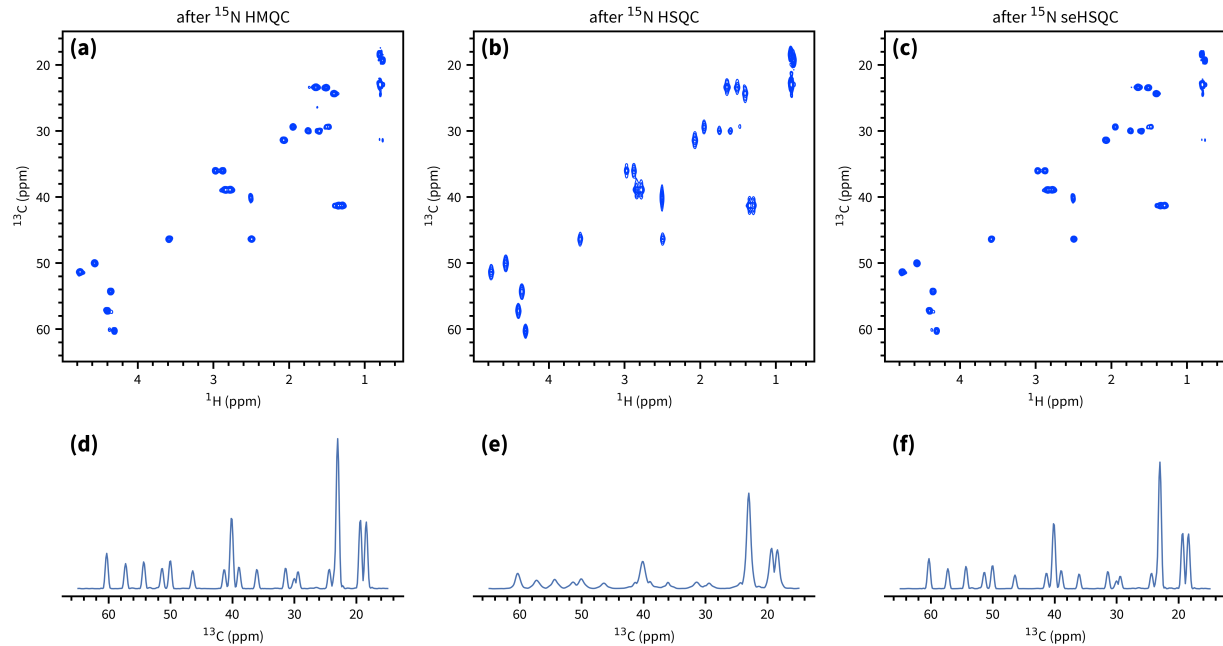


*Figure S7:*  $^{13}\text{C}$  seHSQC spectra obtained from NOAH-3 XSpCc ( $^{15}\text{N}$  module +  $^{13}\text{C}$  seHSQC + CLIP-COSY) supersequences. The  $^{15}\text{N}$  spectral window was 30 ppm and 256  $t_1$  increments were collected, corresponding to an indirect-dimension  $^{15}\text{N}$  acquisition time of 60.1 ms. (a) X = HMQC. (b) X = HSQC. (c) X = seHSQC. (d)–(f) Projections of spectra (a)–(c) onto the  $f_1$  axis. Note the  $f_1$  line broadening in (b) and (e). Spectra were obtained on a 700 MHz Bruker AV III equipped with a TCI H/C/N cryoprobe; the sample used was 40 mM gramicidin in  $\text{DMSO}-d_6$ .

This line broadening also leads to a substantial sensitivity loss (almost 65% in Figure S7). The extent of the line broadening depends on the acquisition time, and is particularly pronounced for long acquisition times, i.e. small  $^{15}\text{N}$  spectral windows. In our experience, at  $^{15}\text{N}$  acquisition times of ca. 5 ms the effect is almost indiscernible. Such a short acquisition time would lead to poor resolution in the  $^{15}\text{N}$  dimension itself, which may or may not be tolerable. Of course, this issue can be entirely avoided by using either the HMQC or seHSQC.

## 7 Effect of lengthened gradients in $^{15}\text{N}$ experiments

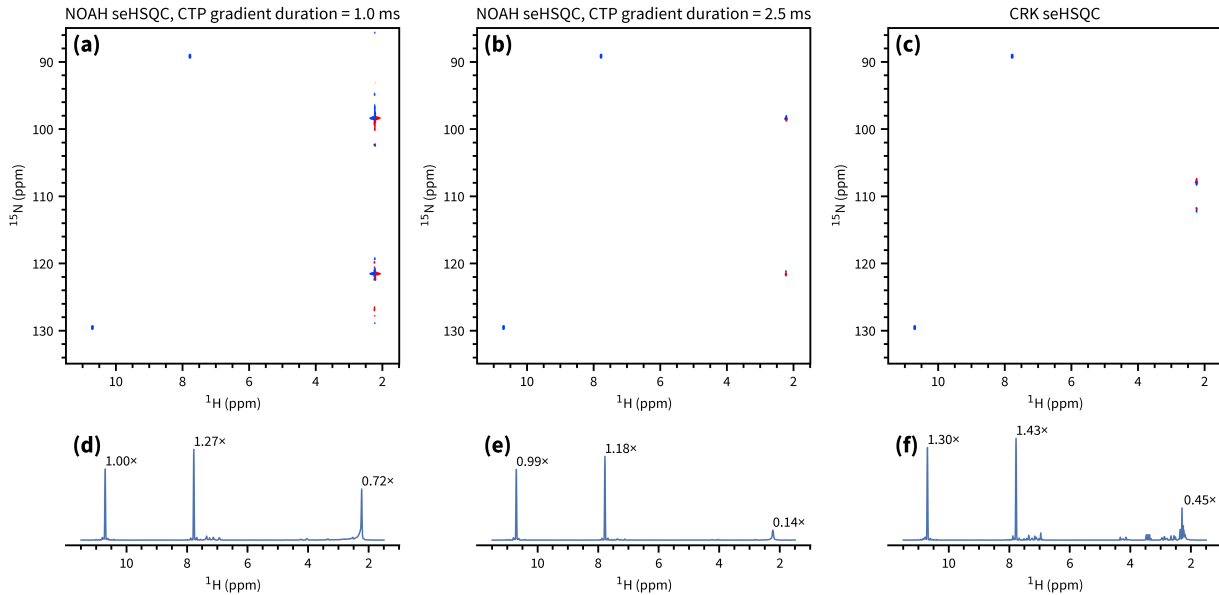


*Figure S8:*  $^{15}\text{N}$  seHSQC spectra obtained using the NOAH and CRK implementations. The peaks at 7.8 and 10.7 ppm ( $^1\text{H}$  shifts) are genuine crosspeaks; the mixed-phase peaks at 2.2 ppm are artefacts. (a) NOAH seHSQC, with original CTP gradients of 1 ms. (b) NOAH seHSQC, with longer CTP gradients of 1 ms. (c) Standalone CRK seHSQC with 1 ms CTP gradients. (d)–(f) Projections of spectra (a)–(c) onto the  $f_2$  axis. The numbers indicate relative peak heights (normalised against the 10.7 ppm peak in (d)). Spectra were obtained on a 700 MHz Bruker AV III equipped with a TCI H/C/N cryoprobe; the sample used was 50 mM zolmitriptan in DMSO- $d_6$ .

The lengthening of CTP gradients from 1 ms to 2.5 ms is aimed at cleaning up artefacts arising from bulk magnetisation that is not properly returned to  $+z$  at the end of the sequence. Figure S8 shows exactly how effective this strategy is. In (d), where the CTP gradients have their original duration, the artefacts have comparable intensity to the desired peaks. When the gradients are lengthened in (e), the crosspeak intensities are almost unaffected (with losses of < 10% arising perhaps from relaxation and diffusion). However, the artefacts are suppressed by a factor of 5 or more. Although this suppression is not complete, this should not be interpreted as a weakness of the new NOAH seHSQC module, as similar artefacts are also visible in the CRK seHSQC (f). Indeed, every  $^{15}\text{N}$ - $^1\text{H}$  experiment we tested has at least *some* artefact intensity in this region.

## 8 Effect of $k$ -scaling

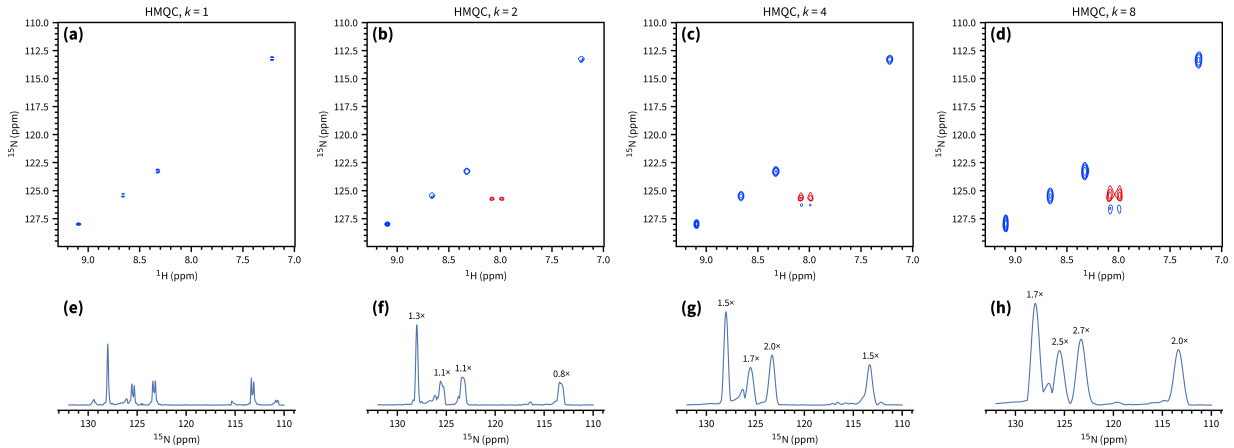


*Figure S9:*  $^{15}\text{N}$  HMQC spectra (from NOAH-3 MSpCc supersequences) obtained with various values of the scaling factor  $k$ . The peak at  $\Omega_{\text{H}} = 8.03$  ppm is a folded peak from the ornithine  $\delta\text{-NH}_2$ . (a)  $k = 1$ , with 256  $t_1$  increments and 2 scans per increment. (b)  $k = 2$ , i.e. effectively 128  $t_1$  increments and 4 scans per increment. (c)  $k = 4$ . (d)  $k = 8$ . (e)–(h) Projections of 2D spectra in (a)–(d) onto the  $f_1$  axis. Numbers indicate peak intensities relative to the  $k = 1$  HMQC spectrum. Spectra were obtained on a 700 MHz Bruker AV III equipped with a TCI H/C/N cryoprobe; the sample used was 40 mM gramicidin in DMSO-*d*<sub>6</sub>. [I don't entirely like the fact that the spectra (and text) are getting a bit small here. I see a few alternatives: (1) stay as is; (2) reduce to three spectra, i.e. remove  $k = 8$ ; (3) change the layout to have 2 spectra and 2 projections per row; (4) only show the 2D spectra and not the projections. This last option is depicted below. Let me know what you think...]

The effect of  $k$ -scaling on the HMQC is shown in Figure S9 (or Figure S10). By decreasing the indirect dimension resolution, the  $f_1$  linewidths of the peaks increase: this can lead to significant sensitivity enhancement for the HMQC (up to 2.7×), because  $J_{\text{HH}}$  splitting in the  $f_1$  dimension is no longer resolved. The largest gains are observed for peaks where  $J_{\text{HH}}$  splitting is more visible; for the leftmost peak at  $\Omega_{\text{N}} = 128$  ppm, only 1.7× gains in sensitivity can be attained through this method.

For the seHSQC module,  $k$ -scaling on its own leads to far smaller sensitivity gains (Figure S11). Any increase in the total peak intensity is almost completely offset by the  $f_1$  broadening. Therefore, even at  $k = 8$ , the largest sensitivity gains that can be attained are  $\sim 1.3\times$ .

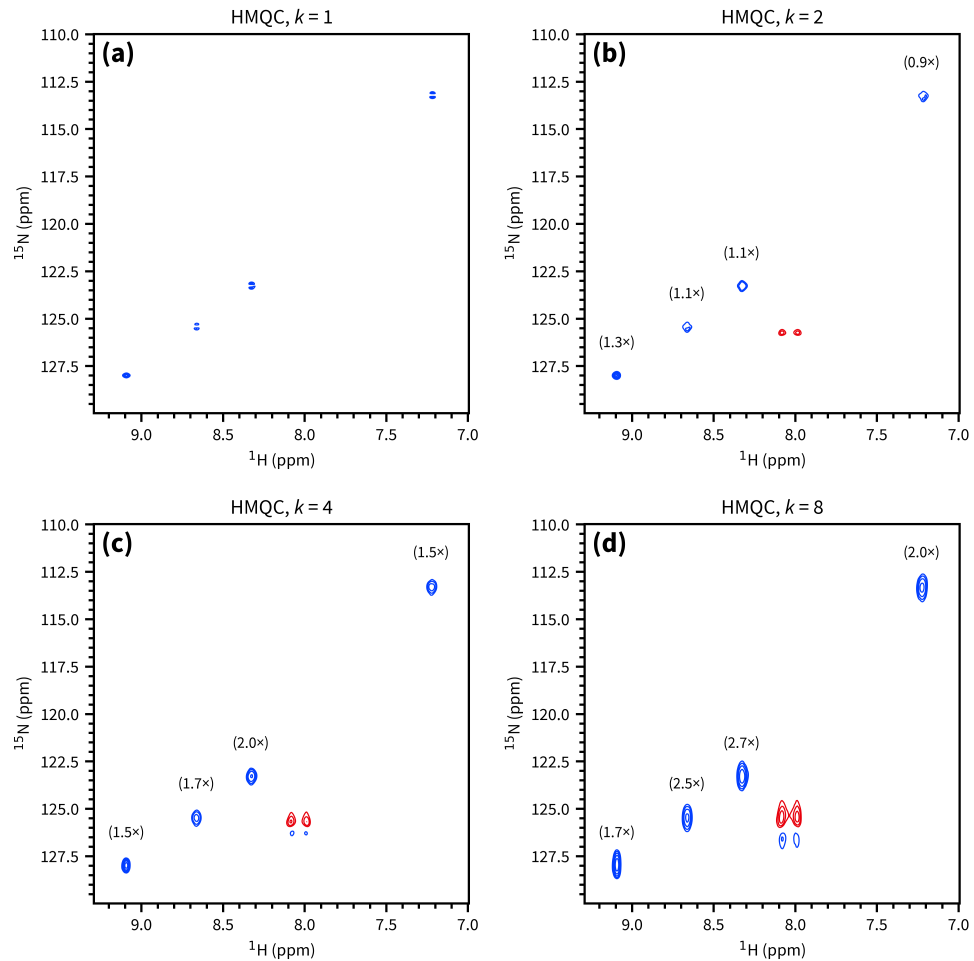
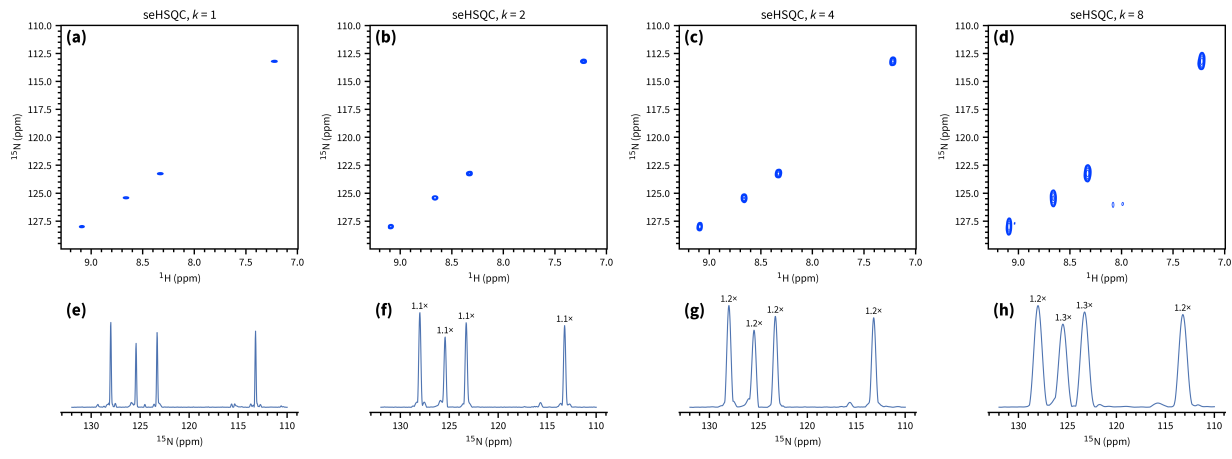


Figure S10: Option 4 as described in the caption of the previous figure.



*Figure S11:* <sup>15</sup>N seHSQC spectra (from NOAH-3 SpSpCc supersequences) obtained with various values of the scaling factor  $k$ . The peak at  $\Omega_H = 8.03$  ppm is a folded peak from the ornithine  $\delta\text{-NH}_2$ . (a)  $k = 1$ , with 256  $t_1$  increments and 2 scans per increment. (b)  $k = 2$ , i.e. effectively 128  $t_1$  increments and 4 scans per increment. (c)  $k = 4$ . (d)  $k = 8$ . (e)–(h) Projections of 2D spectra in (a)–(d) onto the  $f_1$  axis. Numbers indicate peak intensities relative to the  $k = 1$  seHSQC spectrum. Spectra were obtained on a 700 MHz Bruker AV III equipped with a TCI H/C/N cryoprobe; the sample used was 40 mM gramicidin in DMSO- $d_6$ . Same issue here as for the HMQC plot...

## 9 HSQC-TOCSY/HSQC sensitivity comparisons

The signal intensities for the NOAH-3 StSCc (HSQC-TOCSY + HSQC + CLIP-COSY) supersequences can be more conveniently measured by omitting the DIPSI-2 isotropic mixing in the HSQC-TOCSY supersequence, leading to a NOAH-3 SSCc (HSQC + HSQC + CLIP-COSY) supersequence. This allows us to compare the different versions of double-HSQC sequences, as the two HSQC modules can be implemented either using the MFA approach, or the new ASAP/NOAH approach based on Ernst angle excitation in the first module. In the latter implementation, the parameter  $f$  can be varied between 0.4 and 1; it represents the proportion of  $^{13}\text{C}-\text{H}$  magnetisation used in the first HSQC, as described in the main text. Furthermore, to boost the sensitivity of the second HSQC module in the NOAH supersequences, the new seHSQC module can be used in place of it.

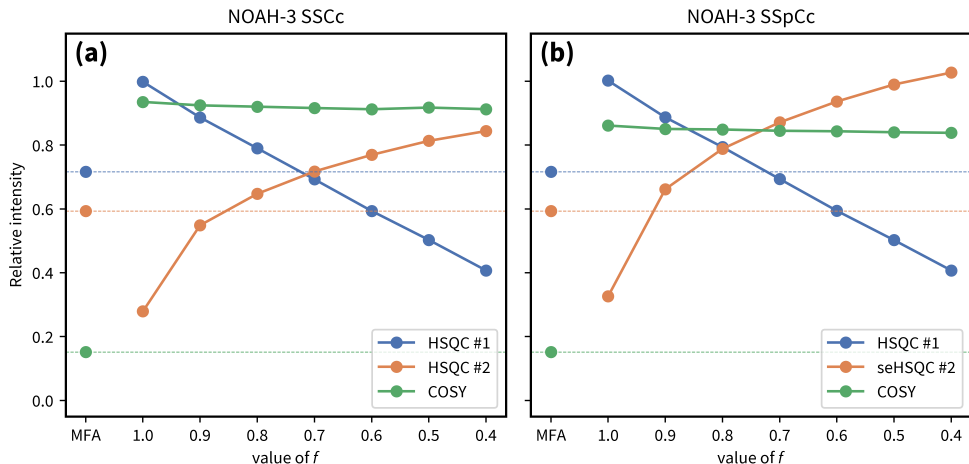


*Figure S12:* Sensitivities of HSQC and CLIP-COSY modules when used as part of a SSCc-type supersequence, with both the NOAH and MFA implementations of the two HSQC modules. Intensities are calculated relative to the HSQC and CLIP-COSY modules in a standard NOAH-2 SCc supersequence (averaged over all peaks). The MFA SSCc sensitivities are on the left of each plot; horizontal dashed lines at these levels are drawn to guide the eye. (a) Sensitivity of NOAH-3 SSCc modules as a function of  $f$ . (b) Sensitivity of NOAH-3 SSpc modules (the second HSQC module is replaced with seHSQC) as a function of  $f$ . Spectra were obtained on a 700 MHz Bruker AV III equipped with a TCI H/C/N cryoprobe; the sample used was 40 mM andrographolide in  $\text{DMSO}-d_6$ .

Figure S12 can be understood in the following way:

- The MFA HSQC sensitivities (on the left of both plots) are approximately half that of a standard CRK seHSQC, with the second HSQC having slightly lower sensitivity. This is discussed in ref. (15) of the main text.
- The sensitivity of the first NOAH HSQC (blue) is generally exactly equal to  $f$ , supporting the interpretation of  $f$  as the fraction of  $^{13}\text{C}-\text{H}$  magnetisation excited in the first HSQC.

- The sensitivity of the second NOAH HSQC (orange) arises from whatever is *not* used by the first HSQC, plus any magnetisation that relaxes during the FID of the first HSQC. As  $f$  is decreased, the former contribution increases and the latter tapers off. This is true for the seHSQC as well (in Figure S12b), except that there is a uniform boost in sensitivity for all values of  $f$ . This sensitivity improvement mainly applies to CH groups, as discussed in the main text.
- The MFA COSY sensitivity is substantially lower ( $\sim 15\%$ ) because the bulk magnetisation is dephased by the previous modules, whereas in the NOAH approach it is (largely) preserved.

(The remainder is quite technical. Should we include it?)

What remains is then to evaluate the impact of adding DIPSI-2 mixing into one of the HSQC modules, to convert it into a HSQC-TOCSY module. In this supersequence, there are three different modules to be investigated. We assume here that in both the MFA and NOAH approaches, the signal intensity of a HSQC-TOCSY module will be directly proportional to the signal intensity of the HSQC module which it is derived from. Therefore, we only need to consider the effect on the COSY (or other homonuclear module) that follows, as well as the *other* HSQC (or seHSQC) module.

1. First, we can consider the effect on the downstream COSY module. This is only really relevant for the NOAH supersequences, where the bulk magnetisation is preserved to begin with. We find that generally the addition of mixing leads to a  $\sim 10\%$  sensitivity loss in the COSY module (independent of the value of  $f$ ), which is still quite tolerable.
2. Then, we can consider the effect on the other HSQC. There are two sub-cases:
  - (a) If the mixing is added to the *second* HSQC module, then the first HSQC module must be unaffected (by causality), and we are done. (Note that, however, causality may not hold if the recovery delay  $d_1$  between scans/increments is too short.)
  - (b) If the mixing is added to the *first* HSQC module, then we need to check how this affects the second HSQC module. This is not possible for the MFA approach, so we need only consider the NOAH approach here. We have a slight problem here now. I have data for HSQC + mixing + HSQC + COSY supersequences where the mixing is applied *between* modules, after the first FID, but not for HSQC-TOCSY + HSQC + COSY supersequences where the mixing is before the first FID. I think it's better to re-acquire the data (I will do so on Saturday), rather than to make the assumption that the effect on the second HSQC will be the same.

## 10 Other example spectra

I want to reacquire some of these with increased HMBC gradients to try and minimise artefacts.

## 11 Pulse programmes

...

## 12 Processing scripts

...